Opto-mechanical analysis of a fast steering secondary mirror prototype for the giant magellan telescope

Myung K. Cho[1], Kwijong Park[2], Young-Soo Kim[2] and Il Kweon Moon[3]

1 National Optical Astronomy Observatory, 950 N. Cherry Ave., Tucson, AZ 85719, USA
2 Korea Astronomy & Space Science Institute, 61-1 Whaam-dong, Yuseong-gu, Daejeon, Korea 305-348
3 Korea Research Institute of Standards and Science, 267 Gajeong-Ro, Yuseong-gu, Daejeon, Korea 305-340
Corresponding Author / E-mail: mcho@noao.edu TEL: +1-520-318-8544, FAX: +1-520-318-8424

KEYWORDS : extremely large telescope, GMT Secondary Mirror, opto-mechanics, mirror support systems, image quality

The Giant Magellan Telescope (GMT) will be a 25m in diameter which is one of the extremely large telescope projects under the design and development phase. The GMT will have two Gregorian secondary mirrors, an adaptive secondary mirror (ASM) and a fast-steering secondary mirror (FSM). Both are 3.2 m in diameter and built as seven circular segments conjugated 1:1 to the seven 8.4m segments of the primary. The baseline configuration of each FSM segment is a lightweight mirror with a 1.06m in diameter, a depth of 140mm and its mass of approximately 100kg. Support system of the lightweight mirror consists of 3 axial actuators, one lateral support at the center, and a vacuum system. The prototype of FSM (FSMP) development effort is led by the Korea Astronomy & Space Science Institute (KASI) with several collaborators in Korea, and the National Optical Astronomy Observatory (NOAO) in USA. The optical image qualities and structure functions for the axial and lateral gravity print-through cases, thermal gradient effects, and dynamic performances will be discussed.

Manuscript received: January XX, 2011 / Accepted: January XX, 2011

NOMENCLATURE

r = a separation between pair positions in structure function
x = a position in OPD calculations
$D(r)$ = structure function as a function of r
$\Phi(x)$ = OPD in a position x
$<\Phi(x)>$ = ensemble average of $\Phi(x)$
f-number = focal length divided by diameter of aperture
arc-seconds = an angle equivalent to 4.86×10^{-6} radians
EE80 = Encircled Energy distribution at a 80% in diameter
ppb = one part per billion (10^{-9})
ZA = Zenith angle (degrees)

1. Introduction

In the design and development of high precision optical instruments, a high fidelity mechanical and optical modeling and analysis is commonly demanding for the performance predictions and evaluations of the systems. The Fast Steering Secondary Mirror (FSM) of the Giant Magellan Telescope (GMT) is one of the next generation extremely large telescope projects under the design and development phase. The FSM consists of seven separated circular segment mirrors, and which are conjugated 1:1 to the segments of the primary mirror. Each lightweight mirror segment of the FSM has a diameter of 1.06 m and a nominal thickness of 140 mm, and each of the segments has a three point axial support and a single lateral support. The axial supports are mounted on the back surface of the mirror and oriented parallel to the optical axis and the lateral support consists of a single flexure located at the mirror's center position. For the optical and mechanical (opto-mechanical) analysis of the GMT Fast Steering Secondary Mirror Prototype (FSMP), the design features of the Magellan Secondary mirror (MM2) and their functions were extensively studied. Several finite element models of MM2 were created and the performances were evaluated. For the FSMP performance predictions, the FSM design of GMT currently under development by the National Optical Astronomy Observatory (NOAO) is assumed as a baseline FSM. Modeling and analysis for the FSM was performed using finite element analysis in I-DEAS™. In the mechanical and optical analyses, different lateral flexure models were developed and evaluated to find a design that provides an acceptable lateral performance in terms of stiffness, strength and elastic stability. Moreover, a flexure model was demonstrated for the thermal analysis of a simplified FSM test assembly. The mirror, bonding layer, lateral flexure and mirror cell were modeled for various thermal conditions including air convections, heat flux loadings, and radiations.

Thermal responses of the test assembly were predicted and the temperature distributions of the entire model were calculated for

sample thermal environments. The thermo-elastic analysis was made to obtain the thermal deformation based on the resulting temperature distributions. The preferred lateral flexure concept is further modified and studied. Structural analyses are conducted in order to estimate the mechanical response of the lateral flexure and the response of the latest and more detailed model of the Fast Steering Mirror. From these analyses, a lateral flexure model was selected to be studied individually and then it was incorporated to a detailed model of the FSM assembly in order to evaluate and assess, at a system-level, the opto-mechanical response of the mirror.

The FSM support system was optimized to meet the requirements defined in "GMT Image Size and Wavefront Error (WFE) Budgets"[4]. Preliminary WFE budget allocation for the FSM mirror figure, from mirror supports, are as follows: 40nm "root mean squared" (RMS) at Zenith and 60nm RMS at 60 degrees elevation. These WFEs are equivalent to the RMS surface errors of 20nm and 30nm at Zenith and at 60 degrees elevation, respectively. These WFE allocations were set to a design goal based on the experiences and opto-mechanical analysis with the similar class of mirrors designed at NOAO. To fulfill the optical and mechanical performance requirements, extensive finite element analyses using I-DEAS^{TM} and optical analyses with PCFRINGE^{TM} have been conducted. Mechanical and optical analyses performed include static gravity induced deformations, natural frequency calculations, and support system sensitivity evaluations. For GMT FSM design and development, NOAO takes a conservative engineering approach and utilize concepts established from the f/11 Secondary Mirror of Magellan telescope, where f/11 is a f-number which is the focal length divided by the diameter of aperture of FSM mirror.

2. FSM Mirror Configuration

The FSM mirror is formed by seven separate, circular segments, and the FSM is a meniscus concave and converts the beam reflected from the f/0.8 Primary Mirror into an f/8 Gregorian beam for the science instruments as shown in Fig. 1. Each lightweight mirror segment has a diameter of 1.06 m and a nominal thickness of 140 mm. Each of the segments has a three point axial support and a single lateral support. The axial supports are mounted on the back surface of the mirror and oriented parallel to the optical axis (z-axis) and the lateral support consists of a single flexure located at the mirror's center position. A design concept of the FSM Cell Assembly developed by NOAO in a collaborative effort with the Korean Astronomy and Space Institution (KASI) is shown in Fig. 2. The FSM Cell Assembly consists of FSM mirror, support system, and the mirror cell. The optical prescription of the GMT secondary mirror in this study has a radius of curvature of 4.3058m, a conic constant of -0.71087, and a segment clear aperture of 1.063m. The optical analysis and the image quality calculations in this paper are based on this prescription.

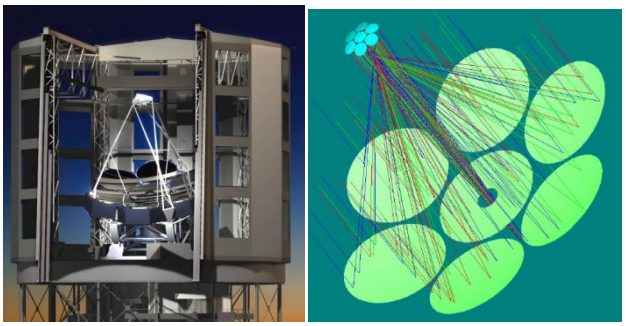

Fig. 1 The GMT telescope artesian model (left) and GMT optics: f/8 Gregorian beams with 1: 1 conjugated Primary and Secondary mirrors (right).

Several different finite element (FE) models were created to serve various calculations. Typical FE mirror model of FSM is composed with four layers of elements with a total of 10,080 solid elements and 12,245 nodes. This model assumes a solid concave lightweight mirror with a diameter of 1.06m, 140mm thick, and a radius of curvature of -4.2m (best fit sphere). The FSM mass was estimated approximately as 100Kg from the solid model shown in Fig. 2. A local coordinate system in the FE model was assumed as follows: (1) the positive Z-axis corresponds to the line which connects the vertex of the primary mirror to the vertex of the secondary mirror in the telescope; (2) the positive X-axis corresponds to the telescope's mechanical elevation axis; (3) the positive Y-axis is defined by the right hand rule. Based on this coordinate system, some of the details of FE results are addresses.

The FSM is designed to meet the FSM image error budget in term of arc-seconds of the encircled energy at a 80% diameter (EE80). These error budgets are give in two extreme telescope orientations and a figure error as: at Zenith, EE80=0.020 arc-seconds; at Horizon, EE80=0.030 arc-seconds; Figure error, EE80=0.039 arc-seconds. One unit in arc-seconds is equivalent to approximately 5 micro-radians. Typical mirror blank material as a baseline assumes Zerodur and its material properties are: Young's modulus: 9.2 x 10^{10} N/m^2, Poisson's ratio: 0.24; Mass density: 2530 kg/m^3, Coefficient of Thermal Expansion (CTE) of Zerodur Class-0, 20 x 10^{-9} m/m/℃ unless specified differently.

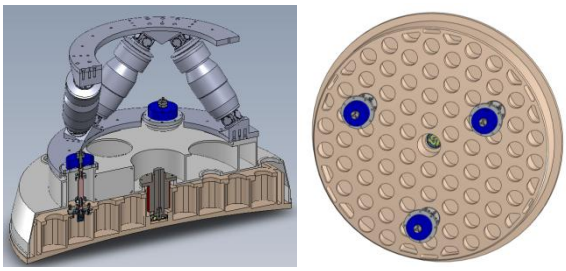

Fig. 2 a design concept of the FSM Cell Assembly consisting of FSM, Support system, and Cell, as shown in a half model at a cut-away view (left); right view shows FSM, Support systems, and hidden Cell. Three axial supports shown in blue, and lateral support mounted at the center of the FSM mirror. The mirror cell is pressurized to balance the mirror gravity.

3. FSM Support System

The baseline mirror support system developed by NOAO contains three (3) axial supports with a tip-tilt capability and a lateral support flexure diaphragm mounted at the center of the mirror as shown in Fig. 2.. This FSM support system was optimized for minimum gravity induced errors. The axial support was optimized for the telescope at Zenith pointing, and the lateral was optimized at Horizon pointing. The optical performance was evaluated for gravity variations between Zenith and Horizon. In addition, support force errors and seal force variations were estimated as a part of the sensitivity and tolerance analyses. To predict the mirror stiffness, fundamental mirror frequencies were calculated with a free-free boundary condition. Detailed mechanical and optical performance analyses were conducted using I-DEAS finite element analysis program and the PCFRINGE optical program.

3.1 Axial Support System

Parametric modeling iterations were conducted for the support system optimization. These iterative calculations utilize an optimization scheme for a minimum global surface deformation over the optical surface. The key metric, during the optimization process, was the optical surface RMS error. In the finite element model, the following design assumptions were made: (1) three axial support (defining points) mounted at the mirror back surface, (2) axial supports oriented parallel to the optical axis (vertical, Z-axis), (3) axial gravity is fully compensated by a vacuum system at Zenith. In

order to achieve the optical performance goal of 20nm RMS surface, extensive parametric calculations were made for an optimum axial support system. The support optimization involves two main optimization processes to achieve the goal; that is, Axial support and Vacuum floating system. The process is as follows: (1) atmospheric pressure was applied on the entire front surface of the FSM from the vacuum, (2) magnitude of the atmospheric pressure set to be equivalent to the axial gravity of FSM, (3) balance the reaction force at the three axial supports to be zero; therefore, the FSM is floating, (4) this floating axial system provides a low surface error in Zenith.

The axial support optimization yields an optical surface RMS error of 3.8nm with a peak-to-valley (P-V) of 21nm. The optical surface contour map for the optimized axial support is shown in Fig. 3(a).

3.2 Lateral Support System

The design concept of the lateral support system was mainly based on the heritage of the Magellan telescope. The FSM baseline lateral support configuration developed by NOAO is a flexure diaphragm mounted at the center hole of the FSM. Current baseline flexure configuration is a diameter of 100mm, a central hub of 32mm with a thin flexure blade thickness of 0.4mm. Extensive trade studies on the center flexure are being performed for the performance, cost, and risk. Some of the detail results were addressed in Chapter 5.

The line of action of the lateral support force exerted by the mirror gravity lateral support should lie on the mid-plane of the FSM mirror. Any excessive force component of the resultant force will result in upsetting the force balance. In order to achieve the optical performance goal of 20nm RMS surface, extensive parametric calculations were made for an optimum lateral support system. The lateral support optimization was processed based on the following design constraints: (1) FSM gravity is held by a flexure at the mirror center location, (2) Line of action is on the mirror center of gravity (CG) plane, (3) no axial force is to be induced at Horizon.
The optical surface error due to gravity, at horizon pointing position, was optimized for a minimum RMS surface error. The optimized lateral support was obtained with the optical surface error of 31nm, RMS and 110nm, P-V. It was confirmed that no axial forces are measured at the axial supports. The optical surface RMS error can be further reduced to 6.1nm if corrected with piston, tip and tilt. The optical surface map and axial forces from the lateral support optimization are shown in Fig. 3.

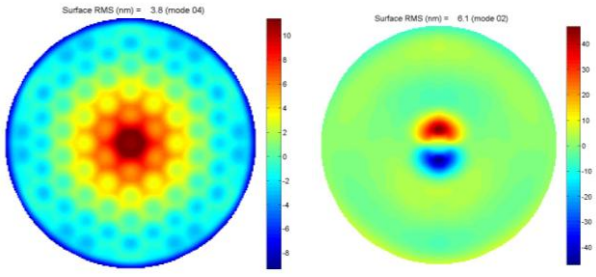

(a) (b)

Fig. 3. FSM support gravity print through error maps; (a) Axial gravity print: (RMS=3.8nm surface), (b) Lateral gravity print through after piston, tip, and tilt corrected (RMS=6.1nm surface).

If FSM mirror was polished, figured, and tested at its face down position at Zenith, then no gravity support error would exist at Zenith. At a 60 degrees Zenith position, the support gravity print through would be a surface RMR of 6nm. The support system adequately meets the optical performance requirements (20nm RMS surface at Zenith and 30nm RMS surface at 60 degrees elevation).

3.3 Support Sensitivity

Sensitivity and tolerance analyses were performed to quantify the optical surface deformations affected by uncertainties in the design and potential errors involved in polishing, assembly and system integration. The analyses include cases such as: axial support force errors, lateral support force errors, and support position errors. As a sample axial support force error mode, considered is a net axial force of 10N at each support location resulting from an unbalanced pressure due to a 97% of the gravity in Zenith. In this case, a RMS error of 4 nm surface was calculated. The optical surface error shows a vivid support print as shown in Fig. 4(a). As another axial support error of interest, force sets exerted by a vacuum seal around the periphery of the mirror were considered. Two extreme force variations, along the optical axis and radial direction, were employed, respectively. As a first case, a uniformly distributed seal force was modeled with an axial force traction (force per unit length) of 10N/m acting on the outer edge of the mirror. This is approximately equivalent to a net axial force of 30N applying to the mirror and no pressure compensation was assumed. In this case, the net change of 12.2nm surface RMS was calculated. Secondly, a uniformly distributed seal force with a radial force traction of 10N/m was applied to the outer edge of the mirror. In this case, the net change of 1.0nm surface RMS was calculated. Current design assumes that FSM performances can be improved by a FSM control system. These seal force errors can be further reduced with a focus correction. The optical surface errors after the focus correction were improved to RMS of 3.9nm and 0.4nm surface, respectively.

The line of action of the lateral support force exerted by the mirror gravity should lie on the mid-plane of the FSM. Any excessive force component of the resultant force will result in upsetting the force balance. As a sensitivity assessment in lateral support, a case in which the lateral support diaphragm is misplaced from its mid-plane along the optical axis was considered. When the lateral diaphragm is misplaced by 1mm along the optical axis, the net change of surface RMS error can be estimated by applying an equivalent load set as a combination of the lateral force and offset moment at the support location. The net changes were calculated with surface RMS of 3.1nm and 1.4nm before and after piston, tip, and tilt corrections, respectively. The optical surface map after the correction is shown in Fig. 4(b).

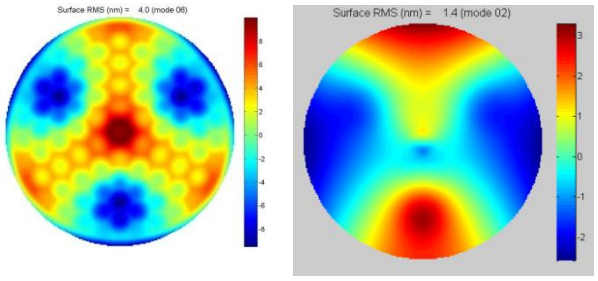

(a) (b)

Fig. 4. Optical surface RMS error maps for support sensitivity cases. (a) Surface error due to the unbalanced axial support force (3% gravity carried by each axial (RMS=4 nm surface); (b) Surface error due to lateral support misplacement of 1mm along the optical axis which shows the net change after piston, tip, and tilt corrected (RMS=1.4nm surface).

4. FSM Mirror Natural Frequency

Natural frequencies of the mirror were calculated by using a solid full FE mirror model with a free-free boundary condition. These frequency modes are characteristic mirror bending shapes and were obtained after removing rigid body motions (piston and tilts). The natural frequencies, up to 22 modes, were calculated and the corresponding characteristic mode shapes were examined. The first 10 characteristic shapes are shown in Fig. 5. The lowest mode was

found at 717 Hz, as an astigmatic shape. The rest low mode shapes up to 10 modes are at 1099, 1411, 1854, 1947, and 2150 Hz. These low frequency modes are similar to low order Zernike polynomials, but not in the same order.

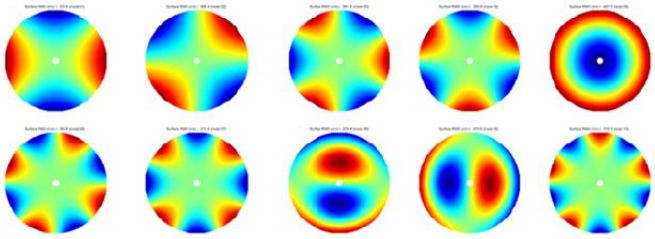

Fig. 5. Mode shapes shown with the first 10 natural mirror mode shapes (free-free).

5. Central Flexure Trade Study

Several lateral support center diaphragm concepts have been studied and analyzed to find a design that provides an optimum structural and thermal performance. Three diaphragm configurations utilized in such analyses are shown in Fig. 6.

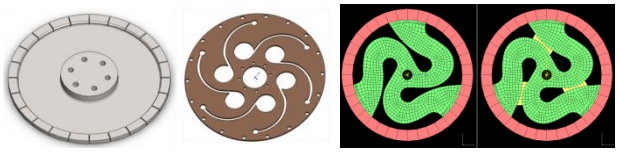

Fig. 6. Three different flexure configurations. Figures from left to right show Configuration-1, Configuration-2 and Configuration-3 (version 3 and 4).

Static and dynamic analyses (linear buckling, geometric nonlinear - large deflections, and frequency) have been performed using each of the three different configurations mentioned above. Such analyses were performed in order to identify which concept provides the optimal amount of axial compliance, while retaining sufficient lateral stiffness, strength, and elastic stability. Summary of some of the results for such analyses is listed in Table 1. Currently, a trade-off analysis is being performed, and more advanced and detailed analyses will be continued as the design evolves.

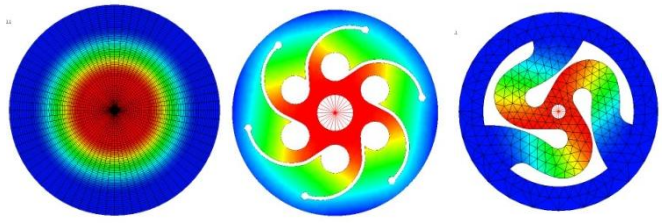

Fig. 6. Typical results for three different flexure configurations.

	Lateral (Load=1000N)		Axial (Disp=1mm)		Bucking	Natural frq.
Flexure Configuration	stiffness (N/um)	Max. Stress (MPa)	stiffness (N/mm)	Max. Stress (MPa)	ratio (Pcr/1000N)	1st mode (hz)
Config 1	196	29	51	180	2.8	500
Config 3 (V4)	110	150	152	973	12.0	980
Config 3 (V3)	16	414	35	333	1.2	377

Table. 1. Lateral flexure performances in different flexure shapes

6. FSM Assembly Thermal Test Model

A finite element model of the Fast Steering Mirror Assembly was created in order to determine its temperature response when subjected to a given thermal environment. The test assembly model consists of three parts: FSM Mirror, the bonding layer and the lateral flexure. The FSM is a low expansion mirror, has a diameter of 200 mm and thickness of 20 mm. The lateral flexure model is a flat diaphragm with a central hub and a slotted outer rim (Configuration 1). The bonding layer is an adhesive material with a thickness of 250 μm. The materials utilized in the analysis and their respective physical and thermal properties are listed in Table 2.

Material	Invar 36 (Flexure)	3M 2216 (Adhesive)	Zerodur (Mirror)
Young's modulus	1.47×10^{11} N/m^2	6.9×10^{8} N/m^2	9.2×10^{10} N/m^2
Poisson's ratio	0.29	0.45	0.24
Density	8050 kg/m^3	1330 kg/m^3	2530 kg/m^3
Conductivity	10.5 W/m℃	0.4 W/m℃	1.46 W/m℃
Specific Heat	515 J/kg℃	1884 J/kg℃	800 J/kg℃

Table 2. Flexure, bonding layer and mirror properties.

As a sample thermal environment and thermal loading condition, a constant heat flux of 5 W/m^2 was applied on the back surface of the mirror and on the lateral flexure. Moreover, air convection with heat transfer coefficients of 5 W/m^2 ℃ and 1 W/m^2 ℃ as well as a time dependent temperature were assumed on the optical and back surfaces of the mirror, respectively. In order to evaluate the thermal response of the FSM Test Assembly for the given thermal environment, a heat transfer analyses was conducted for a combined thermal load with the heat flux, air convection, and radiations. Utilizing the thermal loading condition specified above, the temperature distribution was calculated. The maximum and minimum temperatures obtained for the test assembly are 4.33 ℃ and 3.82 ℃, respectively. The transient thermal response of the mirror is shown in Fig. 7(a). Thermo-elastic analysis was made to calculate thermal deformations. The maximum displacement at time t = 11.5 hrs from the temperature response for the combined loads is 52.5 nm in the test assembly. The thermal deformation is illustrated in Fig. 7(b).

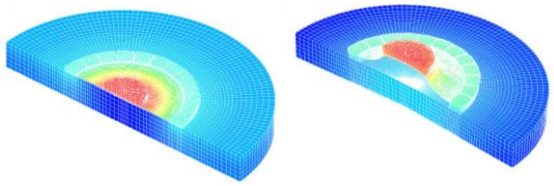

(a) (b)

Fig. 7. Temperature distributions and thermal deformation of test assembly at t = 11.5 hrs, (a) temperature distribution shown in a range from 4.33 ℃ to 3.82 ℃, (b) thermal deformation with a maximum displacement found at 52.5nm.

7. FSM Performance Evaluations

In a seeing limited operation, the FSM optical surface figure errors can be corrected by a fast steering tip-tilt system. For the thermal distortions due to temperature variations on the FSM, FE models were created with a unit thermal gradient of 1^{o}C along each of the local coordinate directions. Modeled, as a most dominant gradient case, was a linear gradient of 1^{o}C along the thickness,1^{o}C/0.1m as a unit case, indicating the top surface is 1^{o}C warmer than the back surface. Furthermore, a CTE of 20 ppb/ ^{o}C was assumed in this thermal gradient case. For this particular case, a P-V surface error of 22 nm and RMS surface error of 6.3 nm were calculated, after removing piston and tilt. Mechanical deformation and the optical surface error maps are shown in Fig. 8. More thermal cases, such as a unit thermal soak, unit gradient along the X axis and Y axis, and radial thermal gradient cases were also examined. The results indicated that these effects are much smaller than that of the gradient case (less than 10%).

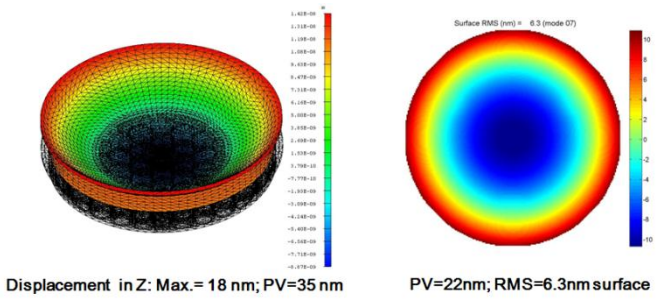

Fig. 8. Thermal deformation due to thermal gradient through the thickness; delta T of 1°C over a thickness of 0.1m; (a) Overall mirror deformation with PV=35nm, (b) the optical surface deformation with RMS surface error of 6.3 nm.

The Image quality analysis was performed for the axial and lateral support print-through from the gravity. For the axial support gravity print-through at Zenith when the axial gravity is fully balanced with vacuum, the Spot diagram and Encircled Energy distribution plot are shown in Fig. 9. The Spot diagram is shown in diameter (arc-seconds). Its Encircled Energy distribution at a 80% (EE80) diameter shows 0.007 arc-seconds.

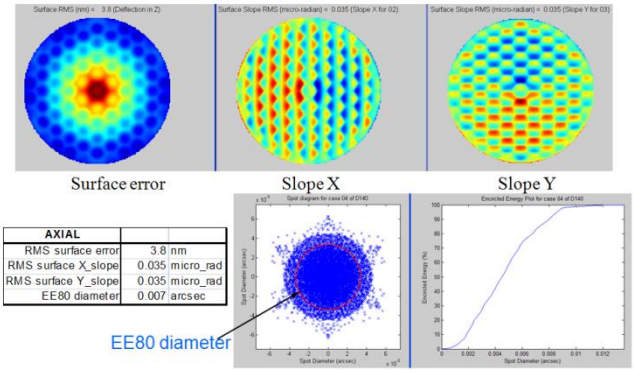

Fig. 9. Image quality analysis of the axial gravity print-through. Top figures show the optical surface map of the gravity support print-through (3.8nm RMS surface) and the corresponding slope errors. Bottom figures show the spot diagram in diameter (arc-seconds) and its encircled energy distribution. EE80 diameter shows 0.007 arc-seconds.

If the secondary mirror was polished, figured, and tested at its face up position, then no gravity support error would exist at the face up position. After the M2 is installed in the telescope, the M2 would be in a -2g axial gravity (reversed gravity impact from null figuring at faced up position) at the telescope in Zenith position. At a 90 degrees Zenith angle (horizon position), the support gravity print-through would be a combination of the axial gravity and lateral gravity errors. Therefore, the resulting surface error becomes 8nm RMS with a quadratic sum of errors from -1g axial (reversed gravity impact) and 1g lateral gravity cases. For the effects on the FSM due to the various Zenith angle (ZA), image quality analysis was performed when the FSM is at ZA of 30 degrees and 60 degrees, respectively. The image quality of the FSM at ZA of 30 degrees shows the gravity support print-through of 3.1nm RMS and the corresponding encircled energy distribution was calculated. Its EE80 diameter shows 0.003 arc-seconds. Similarly, the image quality of the FSM at ZA of 60 degrees is shown in Fig. 10.

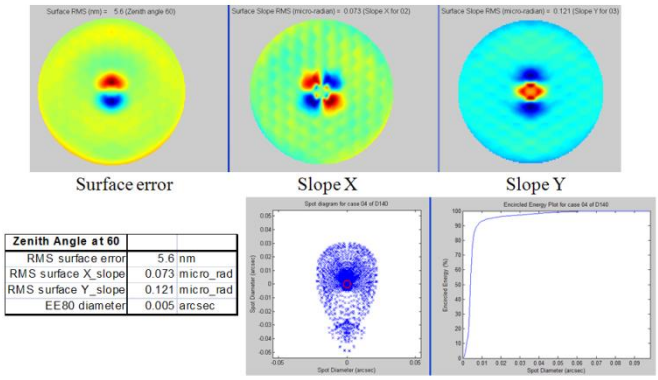

Fig. 10. Image quality analysis at Zenith angle of 60 degrees. Top figures show the optical surface map of the gravity support print-through (5.6nm RMS) and the corresponding slope errors. Bottom figures show the spot diagram in diameter (arc-seconds) and its encircled energy distribution. EE80 diameter shows 0.005 arc-seconds.

In order to control the amplitude of surface figure errors as a function of their spatial frequency, the FSM System Design Requirements Document (DRD) specifies the requirement for surface figure accuracy in terms of an Encircled Energy and a Structure Function (SF). The value of the SF for each separation distance is calculated in terms of the optical path difference (OPD) for each pair of points on the OPD map. SF is defined as:

$$D(r) = < [\Phi(x+r) - \Phi(x)]^2 >$$

where Φ is the OPD at a position x. A SF was calculated for the axial gravity support print-through at all spatial scales and is shown in Fig. 11. For the SF calculation of the FSM, a scale factor of 2 was used to convert the surface error to the OPD. The structure function for gravity print-through was compared to that of the SF requirement in the DRD. The gravity effect is favorably smaller than the requirement by approximately a factor of five.

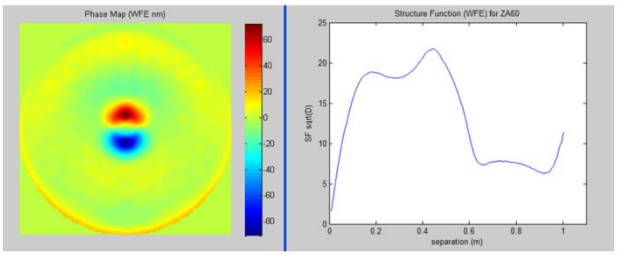

Fig. 11. OPD map of the axial gravity support print-through (10nm RMS surface, or 20nm RMS OPD) and the square root of the structure function, sqrt(D(r)), calculated from the OPD map.

7. Conclusions

Through extensive finite element analyses and optical calculations for an optimized secondary mirror support system of the GMT, a favorable FSM baseline configuration was selected with a diameter of 1.06m; depth of 140mm; face plate thickness of 20mm; and its mass of approximately 100kg. For a favorable lateral flexure design, configuration 1 was selected with an OD of 95mm, ID of 85mm, a diaphragm thickness of 0.5mm. The optimized configuration adequately met the optical performance requirements. The axial support system achieved an optical surface error RMS of 3.8nm with a three-axial actuator support system arranged at a 70% radial position with a balanced vacuum support. The lateral support system was optimized to achieve an optical surface RMS error of 6.2nm. The lateral support system features a diaphragm flexure mounted at the

center of the FSM with the line of action in the mid-plane. The optical surface deformations for various Zenith angles were evaluated by combining cases of the effects from axial and lateral gravities. The results showed that the current GMT FSM mirror support system adequately meets the optical performance goal of 20nm surface RMS in Zenith and RMS of 30nm at 60 degrees, and also satisfies the M2 surface figure accuracy requirement defined in terms of a EE80. That is, for Axial EE80 = 0.007" (< 0.020); Lateral EE80 = 0.005" (< 0.020), and at Zenith angle 60 degrees, EE80 = 0.005" (< 0.039). Sensitivity analyses were conducted with several sample cases to quantify the optical surface deformations affected by uncertainties in design and potential errors involved in polishing, assembly and system integrations. Tip-tilt simulations were performed to capture the impacts from tip-tilt motions. The results indicated that no significant impacts on the mechanical performance in three different flexure configurations.

Integrated FE models with the mirror, supports, and mirror cell structure need to be established for further optimizations to refine design parameters of the mirror cell and support systems. A high fidelity finite element model will be required to evaluate more extensive sensitivity cases, structural interaction effects, thermal mismatches, or other opto-mechanical effects. This FE model may include features of support pads, mounting blocks, linkage, and other detail hardware parts which may contribute to mechanical and optical performance degradation. The depth of FSM should further be confirmed with the GMT optical prescription for the FSM foot print in order not to interfere with the beam path. The lateral diaphragm flexure design and analysis should be continued for the merits among the performance, cost, and risk.

ACKNOWLEDGEMENT

The authors gratefully acknowledge the support of the GMT Office, Matt Johns and Stephen Shectman. This work was partially contributed by the scientists, engineers and students from KASI and KRISS of Korea. Students of The University of Arizona are also greatly acknowledged. The individual contributors are: Ju-Heon Koh, Eun-Kyung Kim, Andrew Corredor, and Christoph Dribusch.

REFERENCES

1. Yoder, P., "Mounting Optics in Optical Instrument", SPIE Press, 2002.
2. Wilson, R., "Fourier Series and Optical Transform Techniques in Contemporary Optics", Willey Interscience, 1995.
3. Cho, M.. and Richard, R.M., "PCFRINGE Program – Optical Performance Analysis using Structural Deflections and Optical Test Data," Version 3.5, the Optical Sciences Center, University of Arizona, 1990.
4. GMT Office, "GMT Image Size and Wavefront Error Budgets", August, 2007.
5. GMT Office, "The F/11 Secondary Mirror of Magellan telescope", August, 2002.
6. Cho, M., "Performance Prediction of the TMT Secondary Mirror Support System", SPIE 7018-65, Marseille, France, 2008.
7. Cho, M., Corredor, A., Park, Kwijong, "K-GMT FSMP PDR", May 6-7, 2010, KASI, Korea.
8. Cho, M., Corredor, A., Park, Kwijong, "K-GMT FSMP PDR-II", November 15-16, 2010, KASI, Korea.
9. Cho, M., Corredor, A., Vogiatzis, K., and Angeli, G., "Thermal Performance Prediction of the TMT Optics", SPIE 7017-43, Marseille, France, 2008.
10. Cho, M., Corredor, A., Vogiatzis, K., and Angeli, G., "Thermal Performance Prediction of the TMT Structure", SPIE 7427-13, San Diego, California, United States, 2009.
11. Blanco, D., Cho, M., Daggert, L., Daly, P., DeVries, J., Elias, J., Fitz-Patrick, B., Hileman, E., Hunten, M., Liang, M., Nickerson, M., Pearson, E., Rosin, D., Sirota, M. and Stepp, L., "Control and support of 4-meter class secondary and tertiary mirrors for the Thirty Meter Telescope," Opt mechanical Technologies for Astronomy, ed. E. Atad-Ettedgui, J. Antebi and D. Lemke, SPIE Proc. 6273, 2006.